journal

J. Am. Ceram. Soc., 99 [5] 1534–1543 (2016)
DOI: 10.1111/jace.14158

Flash Spark Plasma Sintering (FSPS) of α and β SiC

Salvatore Grasso,[‡,§,†] Theo Saunders,[‡,§] Harshit Porwal,[‡,§] Ben Milsom,[‡,§] Adam Tudball,[¶] and Mike Reece[‡,§,*]

[‡]School of Engineering and Material Science, Queen Mary University of London, London E1 4NS, UK

[§]Nanoforce Technology Limited, London E1 4NS, UK

[¶]Kennametal Manufacturing (UK) Ltd., Lake Road Leeway Industrial Estate, Newport, South Wales NP19 4SR, UK

A novel processing methodology that allows combined preheating and Flash-SPS (FSPS) of silicon carbide-based materials has been developed. Beta-SiC (+10 wt% B_4C) powders were densified (Φ 20 mm) up to 96% of their theoretical density in 17 s under an applied pressure of 16 MPa (5 kN). The flash event was attributed to the sharp positive temperature dependence of the electrical conductivity (thermal runaway) of SiC, and a sudden increase in electric power absorption (Joule heating) of the samples after a sufficient preheating temperature (>600°C) was reached. The microstructural evolution was analyzed by examining materials densified by FSPS in the range of 82%–96% theoretical densities. FEM modeling results suggest that the FSPS heating rate was of the order of 8800°C/min. A comparative analysis was done between FSPS and reference samples (sintered using conventional SPS in the temperature range of 1800°C–2300°C). This allowed for a better understanding of the temperatures generated during FSPS, and in turn the sintering mechanisms. We also demonstrated the scalability of the FSPS process by consolidating a large α-SiC disk (Φ 60 mm) in about 60 s inside a hybrid SPS furnace equipped with an induction heater, which allowed us to achieve sufficient preheating (1600°C) of the material to achieve FSPS.

I. Introduction

Flash sintering (FS)[1] provides a new processing route to consolidate materials. While in traditional sintering materials are heated at a relatively slow rate (typically not exceeding 10°C/min) and dwelled for several hours, fully dense materials can be achieved using FS in processing times that are between 10^3 and 10^5 shorter than for conventional sintering. Initial work on FS of zirconia ceramics[2,3] has been followed by research on other materials such as: SnO_2,[4] TiO_2,[5] Y_2O_3,[6] $Ce_xGd_{1-x}O_{1.9}$,[7] Al_2O_3[8], ZnO[9], and SiC.[10] Materials with much higher electrical conductivity such, as ZrB_2[11,12] and $MoSi_2$[11] have also been examined. Modeling[13] and experimental analysis has confirmed[14] that there is a localized heating of the samples due to the Joule effect. It has been reported that the sample temperature might exceed the nominal furnace temperature by more than 1000°C and the process can be explained as a thermal runaway induced by the Joule heating.[15]

Although there is considerable scientific interest in FS, a number of technological issues still remain unsolved:

1. The samples produced so far by FS are typically dog bone shaped,[1] which maximizes the power dissipation. However, this shape does not have any practical application.
2. The sample size (for cylindrical samples) is typically very small (Φ < 5 mm). Scaling up to larger dimensions has not been demonstrated. Thermal gradients and inhomogeneous densification are anticipated issues.
3. The need to preheat the samples makes the process less attractive, especially because the preheating is carried out in conventional furnaces, thus (partially) losing the inherent energy saving benefits of the direct heating. There is therefore a need to integrate the preheating more directly into the rapid processing.
4. Typically, electrodes and connecting wires are made of platinum, which makes the whole process less commercially attractive.

Due to its technological importance and its large production volumes, SiC was selected as an ideal material to demonstrate the feasibility of the FSPS process. Previous work on FS of SiC[10] involved small samples (height 2.5–3.0 mm with a diameter of 5.8 mm) and required the use of a furnace to preheat (at a rate of 5°C/min) the samples to above 1000°C with a dwell time (under discharge) longer than 150 s (overall processing time exceeding 9000 s).

Silicon Carbide based materials are typically densified either by liquid phase or solid-state mechanisms. The densification of additive free SiC has also been reported.[16] To achieve near fully dense materials via solid-state sintering, consolidation of SiC with boron and carbon has been widely investigated. Sintering additives based on B and/or C have been demonstrated to enhance the densification behavior of SiC allowing the formation of fully dense material at a processing temperature of around 2000°C. Boron has been confirmed to reduce significantly the surface energy of the grains,[17] while carbon reduces the amount of residual silica.[18] The properties and preparation route of silicon carbide- and boron carbide-based materials is described extensively in Ref. [19] These composites combine good thermal shock resistance and oxidation resistance. The typical processing route involves pressureless sintering followed by posthiping to produce 100% dense SiC–B_4C, or SPS processing at a temperature of 1950°C under 100 MPa for 5 min.[20]

The aim of this work was to investigate the use of SPS to FS SiC and so avoid the intrinsic limitations of existing FS technology (listed above). Another important difference between flash SPS and conventional flash sintering experiments is the use of pressure in the former. As described in Fig. S1, this work has been divided into two parts, in the first part the feasibility of FS of SiC is demonstrated and

I.-W. Chen—contributing editor

Manuscript No. 37038. Received June 11, 2015; approved January 8, 2016.
*Member, The American Ceramic Society
[†]Author to whom correspondence should be addressed. e-mail: s.grasso@nanoforce.co.uk and s.grasso@qmul.ac.uk

investigated in detail using β-SiC powder (Φ 20 mm, see Fig. S1 Step 2, Route 1), see Section III(*1*). In this work, we demonstrated that conventional SPS equipment (single power source) could be used for flash sintering by replacing the graphite die's with graphite felt. This configuration allowed (a) current flow and Joule heating through graphite felt at low temperature when the sample was still too resistive, thus providing sample heating; and (b) above certain temperature, when the sample resistance falls below that of graphite felt, the current could instead flow through the sample (starting from its outer edge in contact with the felt), thus providing self-Joule heating leading to thermal runaway of the sample. Once (b) began, it behaved just like conventional flash sintering,[21] the only additional elements provided by the SPS equipment is the mechanical pressure and the availability of an enormous amount of current (thousands of Amps) provided under a voltage limit of 10 V.

In the second part, see Section III(*2*), the developed approach is extended to produce large samples using α-SiC powder using a hybrid (dual power source) SPS machine (Φ 60 mm, see Fig. S1 Step 2, Route 2). This was not only to upscale the procedure but also to extend the proposed FSPS process to α-polytype SiC.

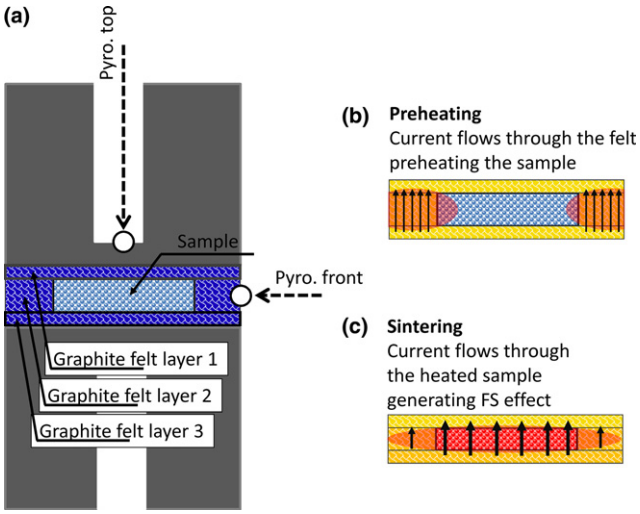

Fig. 1. (a) Experimental setup used to FSPS β-SiC (10 wt% B_4C) in the presence of a graphite felt. (b) The preheating of the sample was achieved with current flowing through the graphite felt. (c) The sintering of SiC was achieved by current flowing through the SiC sample.

II. Experimental Procedure

Both β- and α-SiC were used as starting materials to produce small Φ 20 and large Φ 60 mm samples. The β-SiC was H.C. Starck, Grade BF 12. The powder consisted of 95% β-polytype with the remaining 5% being α. According to the specification provided by the manufacturer, the powder contained in weight % the following elements C 29.5–30.5, O max. 1.5, free Si 0.1, Al max. 0.05, Ca max. 0.01, and Fe max. 0.05 (Si balance). The specific surface area measured by BET (Brunauer–Emmett–Teller) was between 11 and 13 m^2/g. The particle size distribution was D 90% 1.0–2.0 μm, D 50% 0.4–0.9 μm, and D 10% 0.2–0.3 μm. This powder was mixed with 10 wt% B_4C powder, produced by Starck, Grade HD 20, with specific surface area of 22–27 m^2/g. According to the manufacturer, the N, O, Si impurities were 0.7, 2.6, and 0.15 wt%, respectively. The powders were rotary milled in ethanol for 24 h and subsequently dried and sieved. The α-SiC powder was purchased as premixed with sintering additives and was supplied by H.C. Starck Grade Amperpress Alpha UF 15- Premix. The powder contained (in wt%) C 32.5–33.50, B 0.45–0.60, O max 5, Fe max 0.05, Al max 0.04, and Ca max. 0.01 (Si balance).

For the FSPS sintering experiments, the SiC powders were initially precompacted under 16 MPa at 1600°C for 5 min using a SPS machine (FCT HPD 25; FCT Systeme GmbH, Rauenstein, Germany), and then FSPSed in a second step. After precompaction, the density was 50%–55% (depending on the composition of the powder). At this stage, the SiC disks were strong enough to be processed using FSPS.

To perform FSPS, the Φ 20 mm samples were FSPSed using an SPS furnace (FCT HPD 25; FCT Systeme GmbH) under vacuum (~5 Pa). The Φ 60 mm (α SiC) samples were FSPSed in a hybrid SPS machine (H-HP D250; FCT Systeme GmbH). The larger samples were preheated up to 1600°C using induction heating. At these temperatures, the sample was conductive enough and the SPS power (100–200 kW) was applied for a time duration of about 60 s.

In all the FSPS experiments, the temperature was probed by a top pyrometer (focused on the inner graphite wall of the pressing punch at a distance 4 mm from the sample) and side pyrometer [see Fig. 1(a)]. These temperature measurements were used to validate the FEM simulation. In order to minimize the heat loss by radiation from the sample, a graphite felt (GFA5, Sigratherm 6 mm thick flexible carbon felt, SGL carbon group, Wiesbaden, Germany) was wrapped around the SiC sample during sintering. The felt had the usual function of thermally insulating the sample, but also allowed preheating as discussed below. In the FSPS experiments with Φ 20 mm samples, the graphite pressing punches were 50 mm in diameter and height and a constant uniaxial force of 5 kN (16 MPa) was applied. The Φ 20 mm samples were discharged under a peak power of 6–10 kW. A similar configuration was chosen for the Φ 60 mm samples, the pressing punches were Φ 80 mm, and a force of 50 kN (18 MPa) was applied, the SPS peak discharge power was about 90 kW.

Due to the difficulties in measuring the actual sample temperature during the FSPS processing, the process was controlled by limiting the power to a preset value and automatically interrupting the electric power when the displacement reached predetermined values. The temperature history experienced by the sample was derived from microstructural analysis (grain size and density), phase transition (β- α phase transition), and eutectic melting of SiC-B_4C (according to the phase diagram). For comparison, the β-SiC powder mixture was sintered using conventional SPS under a constant pressure of 16 MPa during the entire process. The samples were heated to 1600°C at a rate of 100°C/min and dwelled for 5 min. The temperature was then increased at a rate of 200°C/min and dwelled for 30 s in the temperature range of 1800°C–2300°C. This heating schedule aimed to determine the samples density when processed at high heating rate (i.e., 200°C/min) after being dwelled under precompaction conditions (1600°C for 5 min). The densities of the samples were measured according to ASTM C373-88. Samples were characterized using SEM (FEI, Inspect F, Hillsboro,OR) and XRD (Siemens Diffraktometer-D5000; Munich, Germany).

In order to estimate the temperature conditions experienced by the sample, FEM modeling was employed, as described in Ref. [22] This model included a moving mesh to account for sample shrinkage. In the model, the thermal and electrical properties of the graphite (ISO 63) provided by the manufacturer (Toyo Tanso; Takeshima, Japan) were used. For simplicity, contact resistances were not accounted for and they were lumped into the thermal and electrical conductivities as a function of the temperature of the graphite felt surrounding the sample. The main unknowns in the modeling were the thermal and electrical conductivities of the graphite felt layers. The electrical conductivity of the felt used in the model was 300 S/m and the results generated were matched to the temperature measured by the front pyrometer (preheating stage). The thermal conductivity of the graphite ring

felt surrounding the sample (i.e., not pressed between punches and SiC sample) was provided by the manufacturer and it was normalized (linearly increased according a factor given by the ratio of actual felt height and its initial height). The thermal conductivity of the graphite felt (modeled with thickeness of 2 mm) pressed between the punches and the felt used in the model was constant at 2.7 $W\cdot(m\cdot K)^{-1}$. This value enabled the results to match the temperature measurements recorded by the top and side pyrometers. The temperature-dependent thermal conductivity and specific heat of the SiC materials were taken from the literature.[23] The temperature dependence of the electrical conductivity of SiC was derived by matching the voltage and the temperatures recorded. To obtain more accurate measurements of voltage and current during FSPS, a data logger (National Instruments USB-6221; Newbury, UK) was used. The frequency of the reading was 10 kHZ, and the current was measured by using a National Instrument USB-6221. The voltage was measured between the graphite reducers and current was measured using a Hall effect sensor built into the SPS (ABB, Entrelec NCS125-4 set to high sensitivity mode).

III. Results and Discussion

(1) Φ 20 mm Samples Based on β-SiC, Route 1

Figure 1 show a schematic of the SPS setup used in the present investigation. The setup employs three layers of graphite felt (each 6 mm thick, when not pressed) as top and bottom layers (Φ 40 mm, weight 0.6 g) and a felt ring (OD Φ 40 mm, ID 18 mm weight 0.5 g) hosting the precompacted sample. As summarized in Fig. 1, during the FSPS it is possible to identify a preheating, where current flows through the outer felt [Fig. 1(b)], followed by sintering when current flows through the sample [Fig. 1(c)]. Experiments carried out without graphite felt resulted in no current flowing across the sample, and thus no FSPS event. This is because the minimal current which the SPS machine could supply was of the order of 100 A, and the upper voltage was limited to 10 V. As a result of this, no flow of current was recorded, and the sample was too resistive to be heated. Experiments carried out in different configuration (as the one presented in Fig. 1), where the sample was in direct contact with the pressing graphite punches (e.g., without using graphite felt layers 1 and 3) did not result in a FSPS event. This was because the top and bottom graphite felt layers were essential to reduce the heat exchange (they acted as thermal insulation) and thus maximized the preheating of the sample.

Figure S2(a) shows three photographs of the experimental setup. Figure S2(b) shows a photograph of the flash sintered samples. The samples are crack free even though they were subjected to rapid heating. The presence of the thermally insulating felt around the sample prevented the sample cracking during the heating and cooling stages. Compared to samples processed by conventional SPS with thermal cycling lasting 40–45 min, the FSPS experiments lasted, in total, 47 s. The benefits of FSPS developed in this work compared to pressureless FS include: (1) use of inexpensive graphite electrodes instead of platinum; (2) production of samples of larger volume (10 times bigger)[1]; (3) does not require high voltages (<10 V), which might result in inhomogeneous microstructures as confirmed by experimental observation in Ref. [24]; and (4) effective preheating is achieved using graphite felt.

In FS experiments,[1] typically a maximum voltage is imposed and the current is limited to a preset value. In this work, the FSPS experiments were done by limiting the maximum relative power of the SPS machine. Figs. 2(a) and (b) show output data recorded during FSPS of β-SiC + 10 wt% B_4C samples sintered with preset maximum relative power of 60% and 80%, respectively. The electrical resistance, displacement, electric current, SPS heating power, and front pyrometer temperature (see Fig. 2) are shown. An increase in the set power from 60% to 80% resulted in significantly reduced processing times because the dissipated SPS power reached the maximum values of 6 and 10 kW, respectively. The effective SPS power was dependent on both the electrical resistance of the sample and the set maximum SPS relative power.

In Fig. 2, three stages can be identified. Stage 1 covers the time interval where the current was flowing across the felt and preheating of the samples. At the end of this Stage, the felt resistance reached a plateau (maximum current under the set limited voltage, which is proportional to the set relative power). During Stage 2, the current began to flow through the SiC sample. This is confirmed by the subsequent drop in electrical resistivity and temperature drop as measured on the graphite felt (pyro front). Stage 3 covers the beginning of the completion of the densification as indicated by the displacement curves. As seen in Table II (See below), which refers to sample processed via conventional SPS, Stage 3 started when the sample temperature was higher than 1900°C. In fact above this temperature, the sample density increased from 60% to 74% when the temperature was raised from 1900°C to 2000°C (Table II).

As shown in Fig. 2(a), the electrical resistance sharply decreased during the first 10 s (Stage 1). The resistance was calculated as voltage dived by current as recorded during the experiments by the SPS machine. This was due to the positive temperature dependence of the electrical conductivity of graphite. The felt temperature reached a plateau stabilizing around 1420°C (during the time interval 20–50 s), and the electrical resistance was about 30 mΩ. During the time interval between 50 and 60 s, the resistance suddenly dropped from 27 to 13 mΩ and the SPS power increased, suggesting that some of the current flowed through the sample. The sample processed as described in Fig. 2(a) took about 48 s to achieve the necessary preheating for FSPS, and at this stage, the front pyrometer read a temperature of 1420°C. During Stage 2, the current started to flow through the SiC sample and the SPS power suddenly increased from 1 to 2 kW. During the time interval 60–106 s, increasingly more current flowed through the sample as confirmed by both the continuous resistance drop and SPS power increase. The result was a very fast densification with a peak displacement rate of 13 mm/min at 71 s. A similar behavior of resistance, front pyrometer temperature (≈1400°C), and displacement was observed for the sample parameters recorded during FSPS of the sample sintered with 80% of the preset power [Fig. 2(b)]. In this case, due to the higher power dissipation and maximum temperature, the maximum displacement rate reached 30 mm/min at 36 s.

Table I lists the sintering parameter, the relative density and the SiC polytype for materials processed as described in Fig. 2. As shown, the samples processed under 60% of relative SPS power resulted in higher shrinkage (1.93, 2.18, 2.41 mm) when discharged for longer processing times. In order to understand the rapid resistance drop shown in Figs. 2(a) and (b), the literature on electrical conductivity of SiC materials was reviewed (Fig. 3). It is worth noting that the drop in resistance cannot be attributed to the presence of felt, in fact, when the flash SPS process was attempted in the presence of an electrically insulating sample, a drop in electrical resistance was not observed and similarly no current increase occurred.

Because of their thermoelectric properties, the temperature-dependent electrical conductivity of α- and β-SiC based materials has been well studied. Ohba et al.[25] found that the electrical conductivity of α-SiC composites containing 5% B_4C increased from the room-temperature value of 10 to 550 S/m at 800°C. Due to the *n* and *p* type semiconductor nature of α-SiC and B_4C, the conductivity of the composite material is lower than that of the pure silicon carbide. The high-temperature electrical conductivity of single crystals of α-SiC was measured up to about 2000°C.[26,27] As reported by

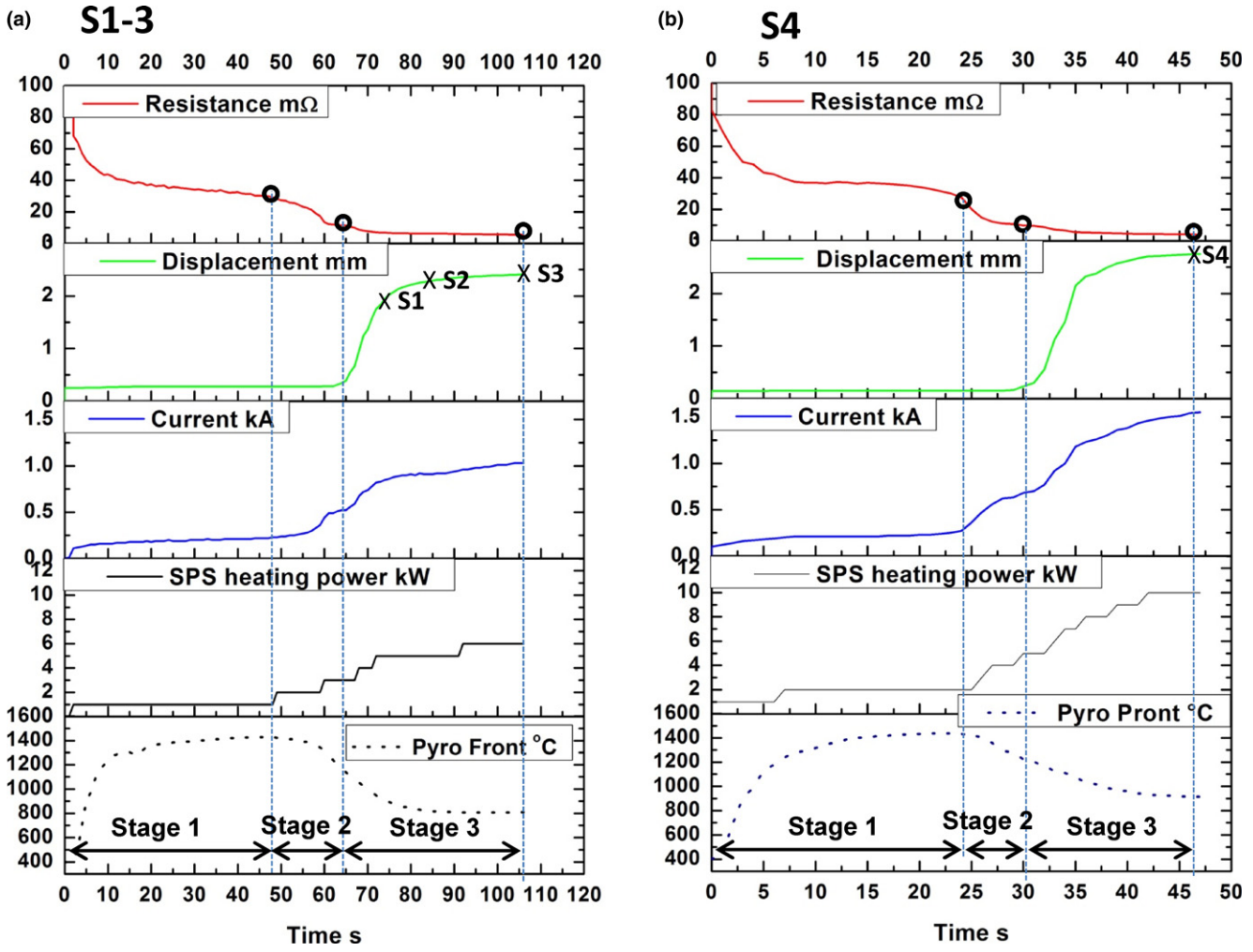

Fig. 2. SPS output data recorded during FSPS of β-SiC (10 wt% B_4C). The set relative power of (a) 60% for sample S1–3, and (b) 80% for sample S4. The electrical resistance, displacement (piston travel), electric current, heating power, and temperature measured on the felt [see Fig. 1(a)] are shown.

Table I. FSPS Condition for the Fabrication of Φ 20-mm β-SiC/B_4C Sample (Step 2, Route 1 see Fig. 1) (Weight 3.4–3.54 g) Listing Shrinkage Reached When the SPS Power was Cut-off, Relative SPS Power, Time Duration from When SPS Current Applied, Time Duration Starting from the Initial Shrinkage of the Sample, Relative Density, and Type of Polytype

Sample label, shrinkage, applied relative power	Total discharge time, Time between shrinkage started (i.e., >0.2 mm) till the end of the discharge process, max SPS power	Relative density and Polytype	Estimated Temperature °C ± 100
Precompacted	Not applicable	53.0%,β	
S1, 1.93 mm, 60%	68 s, 9 s, 5 kW	82.2%, α(4H, 6H)	≈2100°C
S2, 2.18 mm, 60%	73 s, 25 s. 5 kW	88.7%, α(4H, 6H)	≈2200°C
S3, 2.41 mm, 60%	107 s, 43 s, 6 kW	93.2%, α(4H, 6H)	≈2200°C
S4, 2.74 mm, 80%	47 s, 17 s, 10 kW	96.0%, α(4H, 6H)	≈2300°C

Temperature estimated by comparing the density and SiC Polytype of reference samples (Table II). PDF cards; β (01-075-0254), α(4H) (01-073-1663), α (6H) (01-073-1663), Boron carbide (00-001-1163).

Avro et al.[26], the electrical conductivity at 2027°C of single crystal α-SiC was 2000 S/m. Significantly lower electrical conductivities of the order of 500 S/m were reported by Racette,[27] who performed the measurements on six different samples with different purity. As shown in Fig. 3(a), both studies confirmed that the region of intrinsic conductivity was at temperatures above 1400°C–1550°C. At high temperature, the intrinsic electrical conductivity of α-SiC up to about 2000°C has a temperature dependence proportional to $e^{\frac{\Delta E}{2KT}}$, where ΔE is the band gap, K is the Boltzmann constant, and T is the absolute temperature. For reference, the electrical conductivity of α-SiC-based electrical resistor (hot rod heating elements) is also shown in Fig. 3(b).[28]

The electrical conductivity of additive free β-SiC ceramics as a function of temperature was reported by Kitagawa et al.[29] The electrical conductivity of pure β-SiC measured at room temperature was 1.5×10^2 which reached 4.2×10^3 S/m at 800°C. The electrical conductivity reported for β-SiC

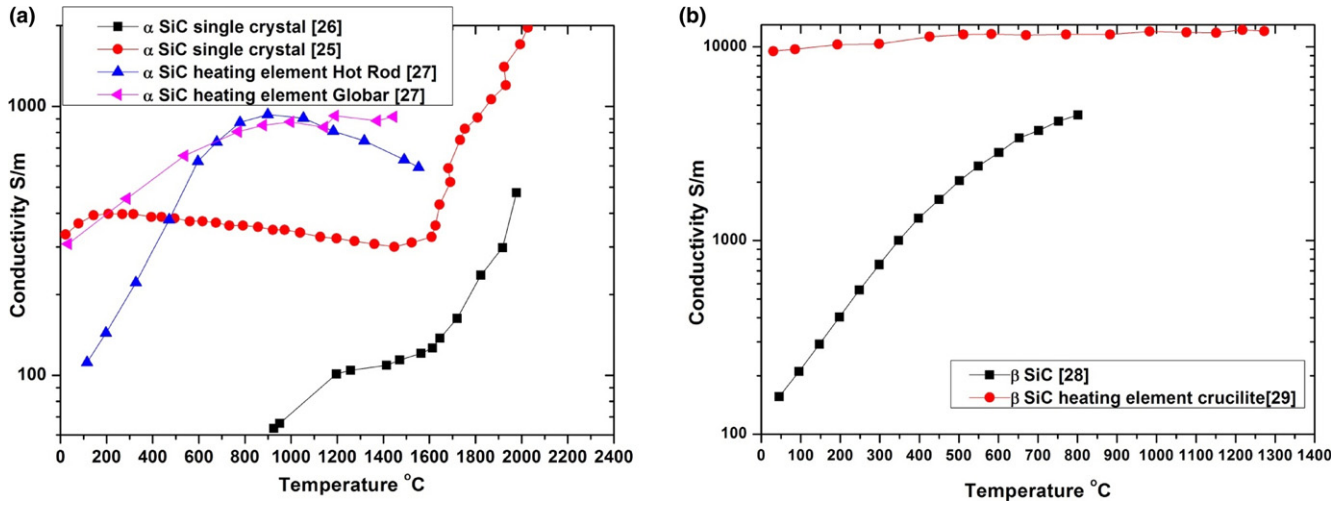

Fig. 3. Electrical conductivity data for (a) α- and (b) β-SiC reported in the literature.

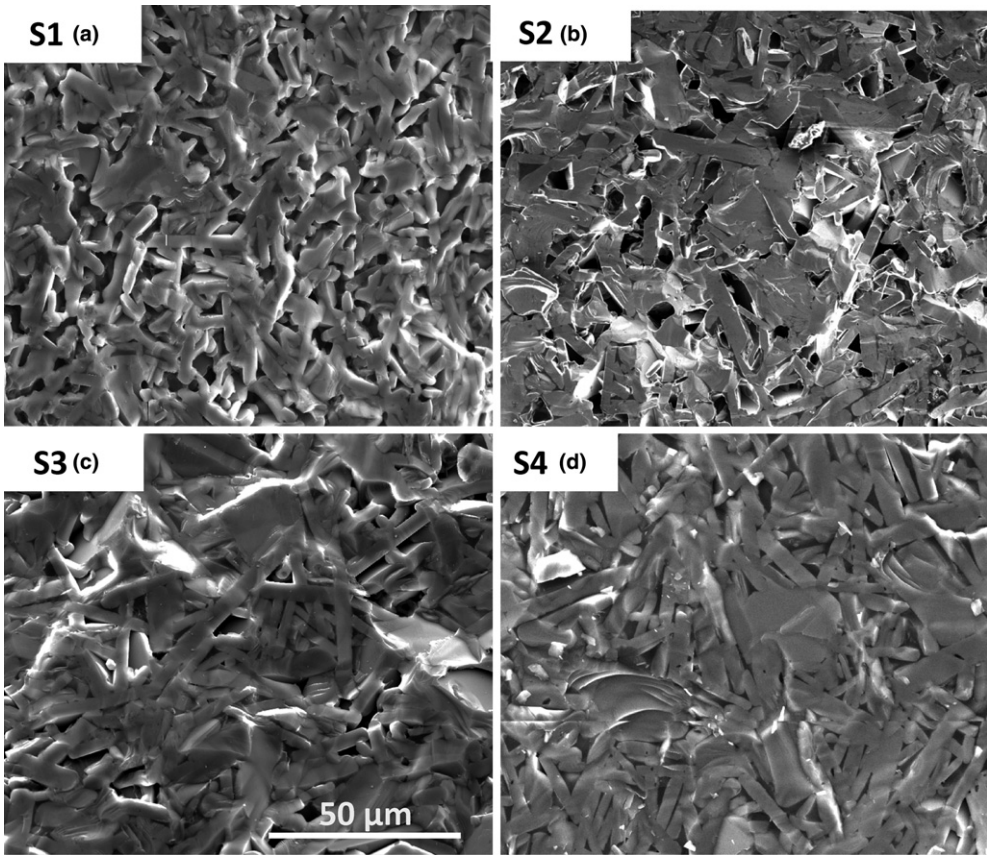

Fig. 4. Fracture surfaces of samples (a) S1, (b) S2, (c) S3, and (d) S4 (β-SiC (10 wt% B_4C)). The images were taken at about the center of the samples at their mid-thickness.

crucilite heating elements is in the range of 0.95–1.2 × 10^4 S/m and is almost temperature independent up to 1500°C.[30] Even though we were not able to accurately measure the electrical conductivity during sintering, the positive temperature dependence of electrical conductivity could explain the FSPS event in terms of thermal runaway phenomena (the progressive increase in electrical conductivity with increasing temperature produced increased Joule heating).

In this study, the electrical conductivity of the graphite tooling was of the order of 10^5 S/m. The electrical conductivity of the β-SiC samples, was at least one order of magnitude lower, this generated direct heating of the sample rather than the graphite tooling. Preliminary results showed that α-SiC could not be FSPSed using the setup shown in Fig. 1. This behavior was attributed to the lower electrical conductivity of the α polytype compared to the β at temperatures below 1000°C as shown in Fig. 3. It is also important to note that the conductivity of the sample during sintering was a function of the temperature and its relative density.

Fracture surfaces of the FSPSed S1–4 samples are shown in Figs. 4(a–d). The figures confirm the density measurements. Figure 4(a) shows evidence of the β-SiC to α-SiC transformation; grain growth and a change in grain shape from equiaxed to high aspect ratio, platelike (lateral size of about 10–20 µm

and height between 3–5 μm) is observed. It is known that β-SiC in the presence of boron results in exaggerated grain growth during the polytype transformation.[31] The resulting microstructure with interlocking platelike grains has been shown to increase the fracture toughness of SiC by crack bridging and crack deflection.[32] The reduced level of porosity and the increased grain size confirm the progressively higher temperature experienced by the samples from S1 to S4, which are estimated in Table I. The S4 samples had larger platelet grains (lateral size up to 50 μm and height between 10–15 μm) compared to S1–3. The boron-rich phase can be seen at the grain boundary.

Table II. Density of Φ 20 mm β-SiC/B_4C Samples Conventionally Sintered (Reference Samples) Dwelled for 30 s in the Temperature range 1800°C–2300°C Under Uniaxial Pressure of 16 MPa (5kN)

Temperature °C (top pyrometer)	Relative density %	Relative density and Polytype
1800	57.8	95% β, 5%α 4H)
1900	60.4	95% β, 5%α 4H)
2000	74.0	95% β, 5% α 4H)
2100	78.2	α(4H) and α (6H)
2200	**97.9**	α(4H) and α (6H)
2300	**97.1**	α(4H) and α (6H)

The powders were poured in a graphite mold and sintered. Bold indicates the highest values.

During the experiments, we attempted to measure the sample temperature by using an optical pyrometer pointed at the sample. However, accurate results could not be achieved because of the presence of radiative surfaces (e.g., not covered by felt to allow temperature measurements with a pyrometer) affected the sample temperature distribution and the sample densities were not comparable with the FSPSed samples (Table I). Considering the rapidity of the sintering process, especially for S4, in order to estimate the sample temperature, the densification and phase transformation behavior of samples prepared using conventional SPS were analyzed.

The densities and polytypes of the samples processed using conventional SPS (reference samples) are given in Table II. The relative density and the β→α phase transformation were used to estimate the temperature experienced by the sample during the FSPS processing. The complete β→α phase transformation occurred when the sample was heated at 2100°C and dwelled for 30 s; for lower temperatures, no significant phase transformation was observed. The transformation temperature range, as reported in the literature, is between 2100°C and 2200°C. Boron is known to decrease the transformation temperature to below 2000°C. It should be noted that the dwelling time in the current work (30 s) was much shorter than those reported in the literature (>10^3 s).[33] As shown in Fig. 5, the precompacted sample processed at 1600°C contained mainly β-SiC, along with (weakly detectable) α-SiC (6H) and boron carbide phases. The samples processed at 1900°C and 2000°C showed slightly increased relative intensities of the α-phase peaks. The phase transfor-

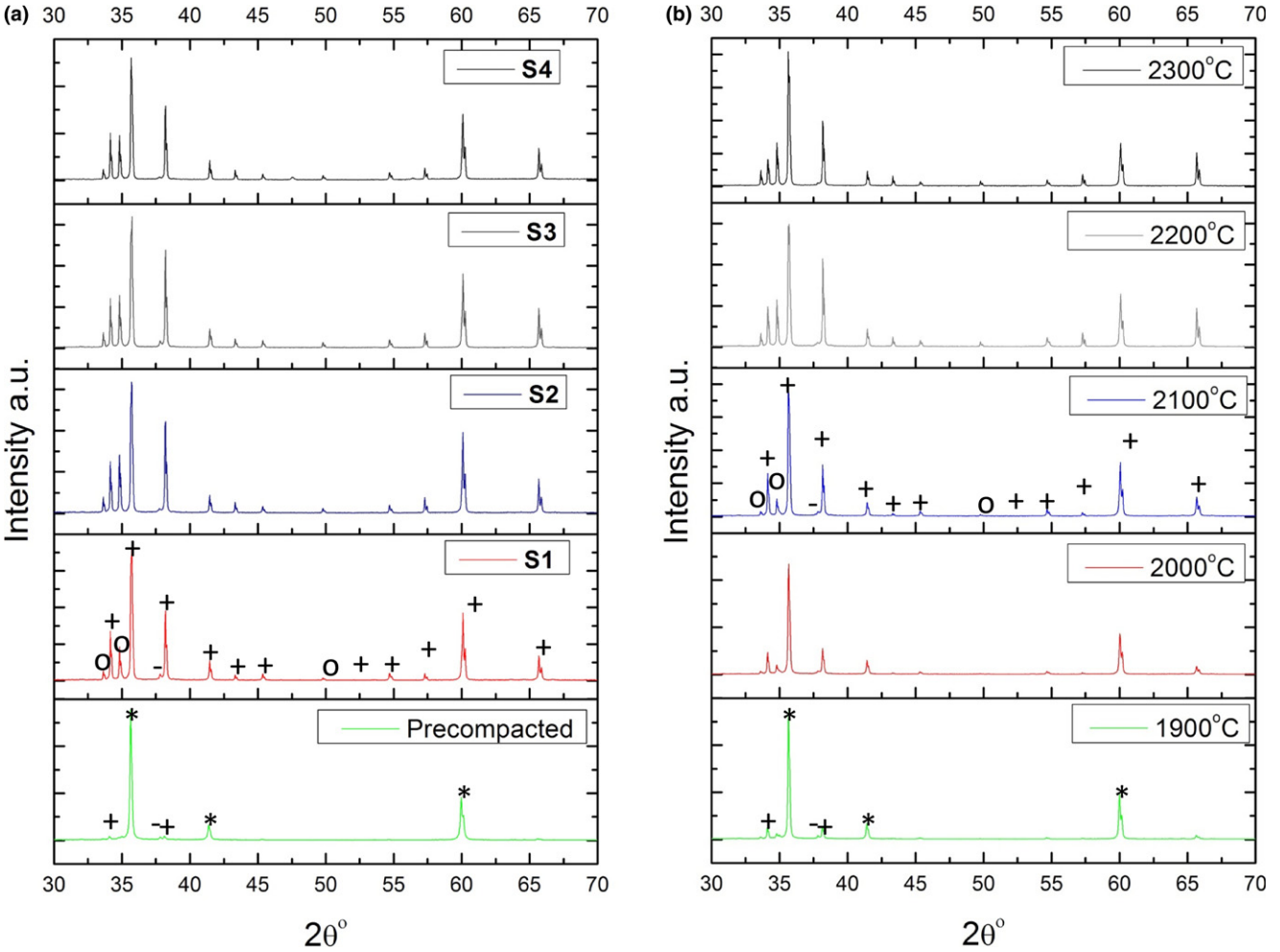

Fig. 5. XRD diffraction patterns for (a) precompacted and FSPSed samples [β-SiC (10 wt% B_4C)] S1–4, and (b) reference samples sintered by conventional SPS in the temperature range 1900°C–2300°C. The symbols * is for β-SiC (0-029-1129), -Boron Carbide (00-001-1163), + SiC (6*H*) (01-073-1663), **o** SiC (4*H*) (01-073-1664).

mation was completed at 2100°C, where the strongest intensity peaks belong to α-SiC (4H and 6H). Compared to the sample processed at 2100°C, samples processed at 2200°C and 2300°C resulted in a stronger intensity of the α-SiC (4H) phase peaks. The 4H-SiC (consisting of stacking planes ABCB…) and 6H-SiC (ABCACB…) are the most common hexagonal polytypes.[34] The results are in agreement with stability diagrams of silicon carbide polytypes described by Knippenberg.[35] According to the results,[35] by increasing the temperature in the range 2000°C–2450°C, the predominant polytype becomes 6H while the 4H fraction decreases. These polytypes have slightly different band gap (3.0 eV for 6H and 3.26 eV for 4H). The decrease in electrical conductivity associated with the β→α phase transformation was not detectable in the resistance curves (Fig. 2),[36] this was mainly because the phase transformation and densification were occurring simultaneously.

The estimated temperature for the FSPS samples is given in Table I (fourth column). The sample S1 with a relative density of 82.2% and mainly consisting of α-SiC (4H, 6H) is comparable with the reference sample processed at 2100°C having a density of 78.2%. The samples S2 and S3, with densities of 88.7% and 93.2% are comparable with the reference samples processed at between 2100°C–2200°C having relative densities in the range 78% and 97%. The lower densities of the FSPS samples compared to reference ones can be attributed to the temperature variation generated in the FSPS process. Since the sample S4 showed the highest density, FEM modeling analysis was performed to determine more accurately the sample temperature distribution during the FSPS process.

The modeled temperature distributions (axial symmetric view) inside the punch/felt/sample assembly are shown in Fig. 6. The temperature distribution after 15 s for the sample S4 is shown in Fig. 6(a). There is good matching between experimental and simulated data, with the surface temperature measured on the surface of the sample ($T_{pyro\ simulated}$ = 1411°C, $T_{pyro\ measured}$ = 1407°C) and voltage drop between the water-cooled rams ($V_{simulated}$ = 6.29 V, $V_{measured\ data\ logger}$ = 6.26 V). At this time instant, the graphite punch temperature was well below the temperature range detectable by the top pyrometer. The arrows indicate the total current density flow in the system. Most of the current traveled across the graphite felt ring [layer 2 in Fig. 1(a)] rather than through the sample. Figure 6(b) shows the temperature distribution at 27 s. There is good matching between experimental and simulated data, with the surface temperature measured on the surface of the sample ($T_{pyro\ front\ simulated}$ = 1422°C, $T_{pyro\ front\ measured}$ = 1358°C) and voltage drop between the water-cooled rams ($V_{simulated}$ = 5.81 V, $V_{measured\ data\ logger}$ = 5.93 V). This time interval is representative of the second stage of the FS process, and the outer region of the sample became conductive after reaching a temperature of about 650°C. This is in agreement with literature data, the electrical conductivity for β-SiC as reported in Ref. [29] at 600°C is as high as 2840 S/m, which is one order magnitude greater than the conductivity of the graphite felt.

Figure 7(a) shows the sample temperature distribution inside the sample at the end of the FS process just before the SPS power was turned off. At this stage, the relatively low temperature (637°C) reached by the graphite tooling suggests that FSPS might not even require water cooling to be integrated in the sintering machines, thus resulting in a simplified design for FSPS machines compared to conventional SPS machines. There is good matching between the experimental and the simulated data, with the temperature measured on the surface of the sample ($T_{pyro\ front\ simulated}$ = 795°C, $T_{pyro\ front\ measured}$ = 913°C; $T_{pyro\ top\ simulated}$ = 643°C, $T_{pyro\ top\ measured}$ = 637°C) and voltage drop between the water-cooled rams ($V_{simulated}$ = 3.40 V, $V_{measured\ data\ logger}$ = 3.53 V). According to the FEM results, the inner part of the sample was hotter than the outer part. This is in agreement with previous modeling work done on conductive materials.[37] The hottest point was located in the center of the sample at its mid-thickness. Due to the sharp difference in the temperature dependence of the electrical conductivity between the SiC and the graphite felt, most of the current flows through the sample, thus generating a radial thermal gradient. As shown in Fig. 7(b), the sharpest radial thermal gradient is observed at a distance 8–10 mm far from the center. This explains the reduced densification reported in this region[37] and the reduced density as shown in supplementary materials (Fig. S3). These FEM results are useful to understand the FS

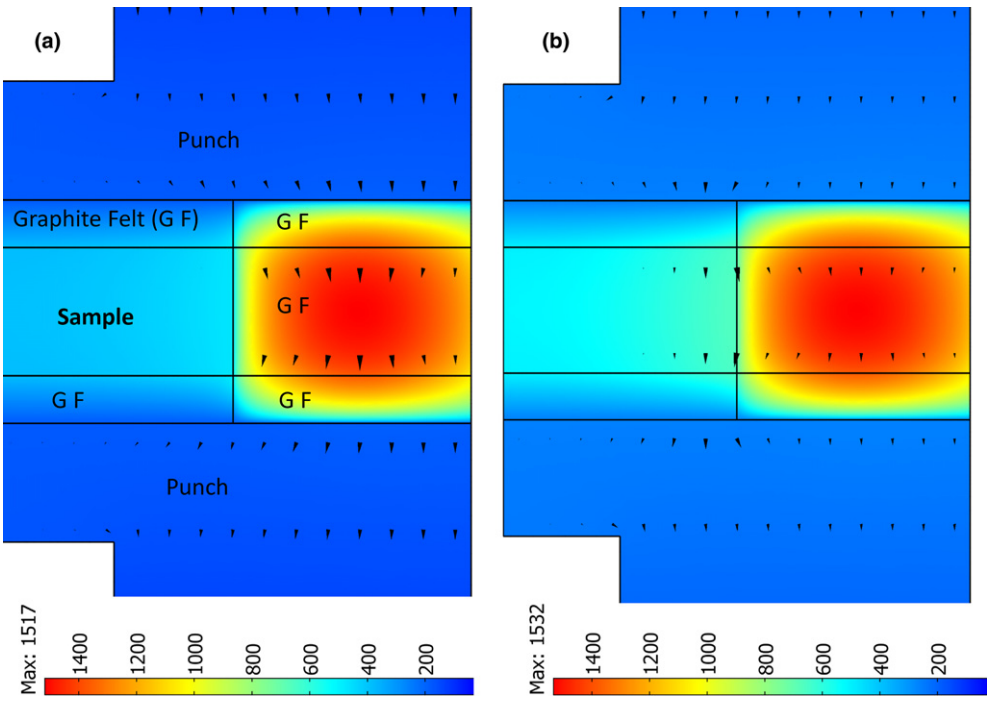

Fig. 6. Simulated temperature distribution (axial symmetric view, °C) inside the punches/graphite felt/sample assembly at times (a) 15 and (b) 27 s during FSPS of β-SiC (10 wt% B_4C). These images are representative of stages 1 and 2, respectively.

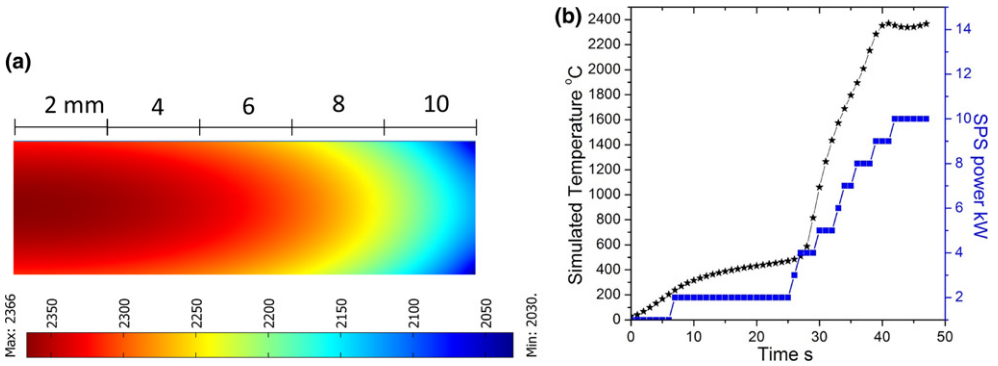

Fig. 7. (a) Simulated temperature distribution (axial symmetric view, °C) inside the S4 SiC sample (β-SiC (10 wt% B_4C) at time 47 s. (b) The simulated sample temperature (sample center and mid thickness) are plotted along with measured SPS power as function of time.

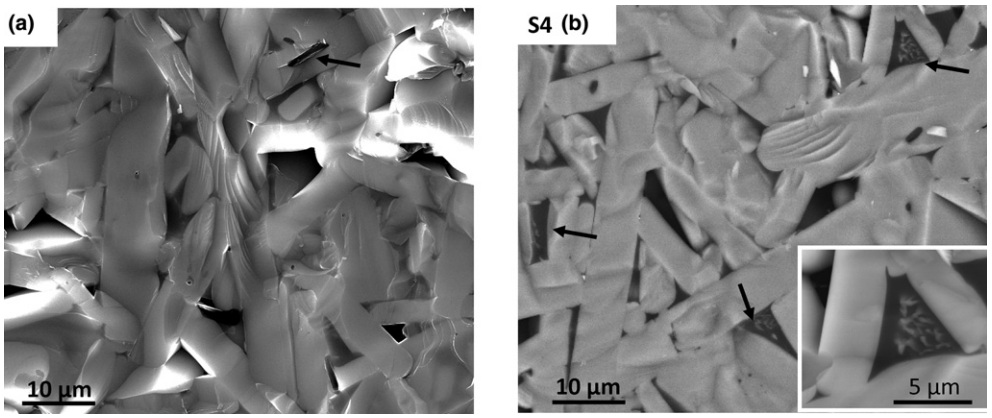

Fig. 8. Fracture surfaces of β-SiC (10 wt% B_4C); (a) refers to the reference sample sintered by conventional SPS at 2300°C for 30 s and (b) sample S4.

process, however, their accuracy might need further validation by using more accurate temperature measurements close to the hottest regions of the sample. The thermal gradients might be reduced by either increasing the preheating temperature, reducing the SPS power, or by developing tooling which allows a current distribution able to promote temperature homogenization inside the sample, as suggested by Giuntini et al.[38]

Figure 7(b) shows the modeled temperature of the sample (center at mid-thickness) and the SPS power as function of the discharge time for sample S4. The top boundary of the sample subdomain was incorporated into a moving mesh to account for displacement. Between the time interval 28–40 s, the heating rate was almost linear and its average was as high as ≈8800°C/minute. As expected, the temperature followed the SPS applied power. In the preheating stage, the sample slowly reached a temperature of about 500°C–600°C and then subsequently FSPSed in just 17 s (see Table II, time interval between 30 and 47 s). The power reached a plateau of 10 kW, and the temperature stabilized at around 2300°C.

As in the case of ZrB_2, FSPS of β-SiC drastically reduced the processing energy and time. Compared to conventional SPS, FSPS of ZrB_2[12] and SiC, to densify a 2-cm diameter sample, resulted in an energy saving of 95% and 99% (to consolidate a precompacted sample), respectively. The greater energy saving, for SiC compared to ZrB_2, is due to the more localized heating (higher electrical resistivity compared to the graphite tooling) which resulted in limited heating of the graphite pressing punches.

Figure 8(a) show the fracture surface of the reference sample sintered by conventional SPS and dwelled for 30 s at 2300°C. In agreement with our previous modeling work,[22] in conventional SPS, we did not observe any significant localized heating (as in the case of FSPS) of the sintering sample. This is mainly because the voltage drop on the sample is reduced by the presence of a graphite mold, which significantly decreases the electrical resistance of the assembly.[39] For comparison, the microstructure of S4 is also shown in Fig. 8(b). The sample S4 shows clearly the presence of some eutectic regions which are highlighted by the black arrows. These regions are not visible in the reference sample, suggesting that the sample S4 might have experienced temperatures in excess of 2300°C. The arrow in Fig. 8(a) indicates graphitic carbon (which is used as sintering additive in the as-received powder). This feature is not observable in Fig. 8(b), which also suggests the S4 sample experienced a higher temperature than the reference sample processed at 2300°C. According to the literature,[40] eutectic melting is observed at 2300°C ± 20°C for the composition 70 ± 2 wt% B_4C and 30 ± 2 wt% SiC. The appearance of a molten eutectic phase supports the modeling results presented in Fig. 8(b).

Unfortunately, by looking at the sintering rates and the power dissipation, there is no means of direct comparison of FSPS with other sintering techniques. This makes elucidation and understanding of the processes/mechanisms difficult. We have attempted to explain the physical mechanisms involved in the rapid densification taking place during FSPS. At the macroscopic scale, an important result from the simulation work is that the sample temperature follows the applied SPS power [Fig. 7(b)], which confirms the thermal run away behavior. On a microscopic scale, in the initial stage of sintering, the densification might be promoted by the formation of hot spots/localized heating at interparticle contact points, as described in Ref. [41] In the second and third stages of sintering, the rapid densification/heating is attributed to quick volumetric mass transport enhanced by two factors (1) the presence of an eutectic molten phases [observed in Fig. 8(b)], promoting a liquid phase sintering and (2) the applied pressure. The activation energy for densification at

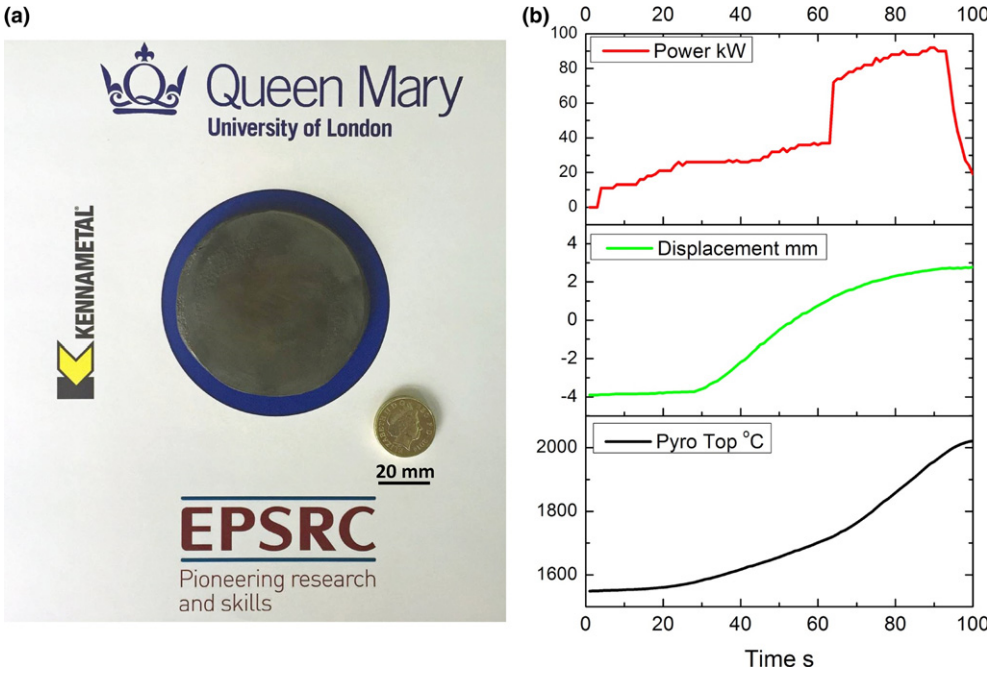

Fig. 9. A photograph (a) of crack free α-SiC crack sample with diameter of 60 mm. (b) SPS data during FSPS performed on a hybrid SPS machine, which allowed preheating of the sample using induction heating. SPS power, displacement (piston travel), temperature measured using the top pyrometer are plotted.

such temperatures has not been reported in the literature.[42] Similarly, it is not possible to achieve such a rapid volumetric heating as in FSPS using other sintering techniques. A comparison for the FSPS runs are the densification curves for samples processed by conventional SPS at 2200°C and 2300°C, and dwelled for 30 s (see Fig. S4 of supplemental materials). At a heating rate of 200°C/min, the displacement reached saturation while heating at a temperature approaching 2250°C. In conclusion, the high temperature reached [Fig. 7(a)] and the formation of a liquid phase [evident for S4, Fig. 8(b)] might be sufficient to explain the rapid densification FSPS. Future work will be focused on establishing the intrinsic electric field contribution (i.e., effects which are not related to the rapid heating) to the rapid densification in terms of accelerated diffusion,[43,46] electro plasticity, or differential heating (within the grains) due the *n* and *p* type semiconductor behavior of the SiC and B_4C.

(2) α SiC- Φ 60 mm

As mentioned in Section III(*1*), α-SiC could not be flash sintered using the experimental configuration shown in Fig. 1. This was mainly due to the lower electrical conductivity of α compared to β at lower temperatures. In fact, the room-temperature electrical conductivity of heating elements [nitrogen-doped α ($1-1.4 \times 10^3$ S/m) and β-SiC ($1-1.4 \times 10^4$ S/m)] differ by at least one order of magnitude.[44] The preheating temperature shown in Fig. 6(b) was not high enough to allow flash sintering of the α-SiC powder employed in this study. In order to overcome this limitation, a hybrid heating mode SPS machine was used. The induction heating allowed preheating of the sample to a temperature of 1600°C and subsequent application of the SPS power. The superposition of direct and indirect heating is termed hybrid heating mode, and was originally developed by Engle in 1940.[45] At present, hybrid heating methods are used for achieving homogeneous densification in SPS when the sample size exceeds 20-cm diameter.

In this section, we show preliminary results on the FS of α-SiC using a hybrid SPS furnace. Similar to what was done in Section III(*1*), the sample was precompacted at 1600°C for 5 min, and the relative density was 52%. After FS, the sample was 98% dense and it was crack free as shown in Fig. 9(a). To the best of our knowledge, this is the largest sample size produced by FS. The production of this sample suggests that FSPS might be scaled up to produce even larger pieces. The electrical parameters recorded during the sintering for α-SiC are shown in Fig. 9(b). The sample was densified (see shrinkage curves) in less than 60 s with an SPS power of about 90 kW.

Conclusions

This work has been the first to demonstrate the densification of SiC-based materials using the novel FSPS route, under conditions in the low-voltage regime (<10 V). Dense β-SiC monoliths (RD = 96%) were manufactured at extremely high heating rate (≈8800°C/min according to modeling results) and short processing times (17 s). The high heating rate (i.e., approaching 10 000°C/min) might allow fabrication of metastable microstructures/compositions in processing cycles which simply cannot be produced by any other technique. We have also demonstrated the upscaling of the technique by producing dense (RD = 98%) and crack-free samples with diameter of 60 mm. This suggests that FSPS might be implemented on an even larger scale, allowing both time and energy saving exceeding 99% when compared to conventional SPS.

Acknowledgments

S.G. was supported by EPSRC (UK EPSRC Material Systems for Extreme Environments programme grant, XMat, EP/K008749/1). T.S. was supported by EC FP7 2007-2013 (ADMACOM). MJR acknowledges the support of the Sunchon National University, South Korea, through the BK21+ programme.

Supporting Information

Additional Supporting Information may be found in the online version of this article:

Fig. S1. Illustration of the processing routes used in this work.

Fig. S2. Photographs showing (a) the processing setup developed for FSPS and (b) processed samples.

Fig. S3. Fracture surfaces of samples S4 (β-SiC (10 wt% B_4C).

Fig. S4. Temperature, displacement, and displacement rate for sample sintered by conventional SPS Φ 20-mm β-SiC (10 wt% B_4C) at (a) 2200°C and (b) 2300°C.

References

[1]M. Cologna, B. Rashkova, and R. Raj, "Flash Sintering of Nanograin Zirconia in <5 s at 850°C," *J. Am. Ceram. Soc.*, **93** [11] 3556–9 (2010).

[2]J. A. Downs and V. M. Sglavo, "Electric Field Assisted Sintering of Cubic Zirconia at 390°C," *J. Am. Ceram. Soc.*, **96** [5] 1342–4 (2013).

[3]R. Muccillo and E. N. S. Muccillo, "An Experimental Setup for Shrinkage Evaluation During Electric Field-Assisted Flash Sintering: Application to Yttria-Stabilized Zirconia," *J. Eur. Ceram. Soc.*, **33** [3] 515–20 (2013).

[4]R. Muccillo and E. N. S. Muccillo, "Electric Field-Assisted Flash Sintering of tin Dioxide," *J. Eur. Ceram. Soc.*, **34** [4] 915–23 (2014).

[5]S. K. Jha and R. Raj, "The Effect of Electric Field on Sintering and Electrical Conductivity of Titania," *J. Am. Ceram. Soc.*, **97** [2] 527–34 (2014).

[6]H. Yoshida, Y. Sakka, T. Yamamoto, J. M. Lebrun, and R. Raj, "Densification Behaviour and Microstructural Development in Undoped Yttria Prepared by Flash-Sintering," *J. Eur. Ceram. Soc.*, **34** [4] 991–1000 (2014).

[7]T. Jiang, et al., "Understanding the Flash Sintering of Rare-Earth-Doped Ceria for Solid Oxide Fuel Cell," *J. Am. Ceram. Soc.*, **98** [6] 1717–23 (2015).

[8]J. Gonzalez-Julian and O. Guillon, "Effect of Electric Field/Current on Liquid Phase Sintering," *J. Am. Ceram. Soc.*, **98** [7] 2018–27 (2015).

[9]C. Schmerbauch, J. Gonzalez-Julian, R. Röder, C. Ronning, and O. Guillon, "Flash Sintering of Nanocrystalline Zinc Oxide and its Influence on Microstructure and Defect Formation," *J. Am. Ceram. Soc.*, **97** [6] 1728–35 (2014).

[10]E. Zapata-Solvas, S. Bonilla, P. R. Wilshaw, and R. I. Todd, "Preliminary Investigation of Flash Sintering of SiC," *J. Eur. Ceram. Soc.*, **33** [13–14] 2811–6 (2013).

[11]E. Zapata-Solvas, D. Gómez-García, A. Domínguez-Rodríguez, and R. I. Todd, "Ultra-Fast and Energy-Efficient Sintering of Ceramics by Electric Current Concentration," *Sci. Rep.*, **5**, 8513 (2015).

[12]S. Grasso, et al., "Flash Spark Plasma Sintering (FSPS) of Pure ZrB2," *J. Am. Ceram. Soc.*, **97** [8] 2405–8 (2014).

[13]S. Grasso, et al., "Modeling of the Temperature Distribution of flash sintered Zirconia," *Nippon Seramikkusu Kyokai Gakujutsu Ronbunshi/J. Ceram. Soc. Jpn*, **119** [1386] 144–6 (2011).

[14]J. Park and I. W. Chen, "In Situ Thermometry Measuring Temperature Flashes Exceeding 1,700°C in 8 mol% Y2O3-Stablized Zirconia Under Constant-Voltage Heating," *J. Am. Ceram. Soc.*, **96** [3] 697–700 (2013).

[15]R. I. Todd, E. Zapata-Solvas, R. S. Bonilla, T. Sneddon, and P. R. Wilshaw, "Electrical Characteristics of Flash Sintering: Thermal Runaway of Joule Heating," *J. Eur. Ceram. Soc.*, **35** [6] 1865–77 (2015).

[16]T. S. Suzuki, T. Uchikoshi, and Y. Sakka, "Densification of SiC by Colloidal Processing and SPS Without Sintering Additives," *Adv. Appl. Ceram.*, **113** [2] 85–8 (2014).

[17]L. Stobierski and A. Gubernat, "Sintering of Silicon Carbide II. Effect of Boron," *Ceram. Int.*, **29** [4] 355–61 (2003).

[18]L. Stobierski and A. Gubernat, "Sintering of Silicon Carbide I. Effect of Carbon," *Ceram. Int.*, **29** [3] 287–92 (2003).

[19]C. Schmalzried and K. A. Schwetz, "Silicon Carbide- and Boron Carbide-Based Hard Materials," in *Ceramics Science and Technology*. Vol. **2**, Edited by R. Riedel, I. -W. Chen. Wiley-VCH Verlag GmbH & Co. KGaA, Weinheim, Germany, 2013.

[20]A. Maître, A. V. Put, J. P. Laval, S. Valette, and G. Trolliard, "Role of Boron on the Spark Plasma Sintering of an α-SiC Powder," *J. Eur. Ceram. Soc.*, **28** [9] 1881–90 (2008).

[21]R. Raj, M. Cologna, A. L. G. Prette, V. M. Sglavo, and J. Francis, "Methods of Flash Sintering"; in Google Patents, 2015.

[22]G. Maizza, S. Grasso, and Y. Sakka, "Moving Finite-Element Mesh Model for Aiding Spark Plasma Sintering in Current Control Mode of Pure Ultrafine WC Powder," *J. Mater. Sci.*, **44** [5] 1219–36 (2009).

[23]A. Rashed, *Properties and Characteristics of Silicon Carbide*. POCO Graphite Inc., Decatur, TX, 2002.

[24]M. C. Steil, D. Marinha, Y. Aman, J. R. C. Gomes, and M. Kleitz, "From Conventional ac Flash-Sintering of YSZ to Hyper-Flash and Double Flash," *J. Eur. Ceram. Soc.*, **33** [11] 2093–101 (2013).

[25]Y. Ohba, T. Shimozaki, and H. Era, "Thermoelectric Properties of Silicon Carbide Sintered With Addition of Boron Carbide, Carbon, and Alumina," *Mater. Trans.*, **49** [6] 1235–41 (2008).

[26]D. D. Avrov, A. S. Bakin, S. I. Dorozhkin, A. O. Lebedev, and V. P. Rastegaev, "Electrical Conductivity of Single-Crystalline Bulk 6H-SiC and Epitaxial Layers of AIN in the Temperature Range 300-2300 K, **264–268**, 521–4 (1998).

[27]J. H. Racette, "Intrinsic Electrical Conductivity in Silicon Carbide," *Phys. Rev.*, **107** [6] 1542–4 (1957).

[28]K. Motzfeldt, *High Temperature Experiments in Chemistry and Materials Science*." John Wiley & Sons, Chichester, UK, 2012.

[29]H. Kitagawa, N. Kado, and Y. Noda, "Preparation of N-Type Silicon Carbide-Based Thermoelectric Materials by Spark Plasma Sintering," *Mater. Trans.*, **43** [12] 3239–41 (2002).

[30]G. G. Gnesin, V. K. Zakharenkov, and L. A. Shipilova, "Volume Electrical Resistivity of Silicon Carbide Heating Elements," *Sov. Powder Metall. Metal Ceram.*, **17** [1] 72–6 (1978).

[31]C. A. Johnson and S. Prochazka, "Microstructures of Sintered SiC"; pp. 366–78 in *Ceramic Microstructures 1976*, Vol. **1**, Edited by R. M. Fullrath and J. P. Pask. Westview Press, Boulder, CO, 1977.

[32]N. P. Padture and B. R. Lawn, "Toughness Properties of a Silicon Carbide With an in Situ Induced Heterogeneous Grain Structure," *J. Am. Ceram. Soc.*, **77** [10] 2518–22 (1994).

[33]Y. Kurata, K. Ikawa, and K. Iwamoto, "The Effect of Heat Treatment on Density and Structure of SiC," *J. Nucl. Mater.*, **92** [2–3] 351–3 (1980).

[34]W. H. Backes, P. A. Bobbert, and W. van Haeringen, "Energy-Band Structure of SiC Polytypes by Interface Matching of Electronic Wave Functions," *Phys. Rev. B*, **49** [11] 7564–8 (1994).

[35]W. F. Knippenberg, *Growth Phenomena in Silicon Carbide*. Vol. **13**. Philips Research. Reports, Valkenburg, 1963.

[36]J. Stęszewski, A. Jakubowski, and M. L. Korwin-Pawlowski, "Comparison of 4H-SiC and 6H-SiC MOSFET IV Characteristics Simulated With Silvaco Atlas and Crosslight Apsys," *J. Tel. Inform. Technol.*, **3**, 93–5 (2007).

[37]G. Maizza, S. Grasso, Y. Sakka, T. Noda, and O. Ohashi, "Relation Between Microstructure, Properties and Spark Plasma Sintering (SPS) Parameters of Pure Ultrafine WC Powder," *Sci. Technol. Adv. Mater.*, **8** [7–8] 644–54 (2007).

[38]D. Giuntini, J. Raethel, M. Herrmann, A. Michaelis, and E. A. Olevsky, "Advancement of Tooling for Spark Plasma Sintering," *J. Am. Ceram. Soc.*, **98** [11], 3529–37 (2015).

[39]S. Grasso and Y. Sakka, "Electric Field in SPS: Geometry and Pulsed Current Effects," *Nippon Seramikkusu Kyokai Gakujutsu Ronbunshi/J. Ceram. Soc. Jpn*, **121** [1414] 524–6 (2013).

[40]D. Secrist, "Phase Equilibria in the System Boron Carbide-Silicon Carbide," *J. Am. Ceram. Soc.*, **47** [3] 127–30 (1964).

[41]T. Saunders, S. Grasso, and M. J. Reece, "Plasma Formation During Electric Discharge (50V) Through Conductive Powder Compacts," *J. Euro. Ceram. Soc.*, **35** [3] 871–7 (2015).

[42]D. A. Ray, S. Kaur, R. A. Cutler, and D. K. Shetty, "Effect of Additives on the Activation Energy for Sintering of Silicon Carbide," *J. Am. Ceram. Soc.*, **91** [4] 1135–40 (2008).

[43]R. Raj, M. Cologna and J. S. C. Francis, "Influence of Externally Imposed and Internally Generated Electrical Fields on Grain Growth, Diffusional Creep, Sintering and Related Phenomena in Ceramics," *J. Am. Ceram. Soc.*, **94** [7] 1941–65 (2011).

[44]M. McIver, H. Seaton, S. Moug, and J. Beatson, "Electrical Resistance Heating Element"; in Google Patents, 2011.

[45]E. W. Engle, "Method and Apparatus for Making hot Pressed Hard Metal Compositions"; US Patent 2,195,297, 1940.

[46]E. Olevsky and S. Rolfing, *Flash spark-plasma sintering of SiC powder: New developments*. MS&T 2014; Pittsburgh, PA, October 2014 (1 p. abstract). □